23rd ABCM International Congress of Mechanical Engineering
December 6-11, 2015, Rio de Janeiro, RJ, Brazil

HIGHER ORDER SPECTRAL ANALYSIS OF ADDED MASS FORCES ON PLUNGING AIRFOIL AT HIGH FREQUENCIES

Mohamed Y. Zakaria
Muhammad R. Hajj
Virginia tech, Department of Engineering Science and Mechanics, Blacksburg, VA 24061, USA
zakaria@vt.edu, mhajj@vt.edu

Danial A. Pereira
Flavio D. Marques
Engineering School of São Carlos, University of São Paulo
daniel.almeida.pereira@usp.br, fmarques@sc.usp.br

Abstract. *Experiments are conducted on a NACA 0012 airfoil undergoing plunging oscillations at high frequency and different angles of attack. At extensively high oscillatory frequency and angles of attack, the formulation of the total loads responsible for generating nonconventional lift mechanisms is very difficult to be modeled. Also, extracting the pure aerodynamic loads from the combined measured output signal (inertia, apparent mass, and the aerodynamic circulatory forces) is a harsh task to do. As such, we introduce a dynamic model based on the gain response function to build an added mass model (response force function model with zero undisturbed flow) based on the obtained experimental data. Using the frequency domain through spectral analysis, we construct a response function gain assuming input-output dynamical system. We also use the higher order spectral analysis to investigate the higher-order interactions between the system frequencies which may lead to unconventional lift mechanisms at high operating frequencies and high angles of attack.*

Keywords: *Added mass, higher-order spectral analysis, high angle of attack, unsteady aerodynamics*

1. INTRODUCTION

Unsteady nonlinear aerodynamics of wing sections is of interest in modeling insect and bird-like flights. One aspect of such flights is the added mass effect which has been shown to have significant contributions on the generated loads in these and other applications. Maniaci and Li (2011) found that the added mass effect caused a 3.6 % change in thrust for a rapid pitch case of a wind turbine blade and a change in the amplitude and phase of the thrust for a case with 30^o of yaw. Granlund and Simpson (2007) showed experimentally that the added mass is linearly dependent on the plunging velocity of a three-dimensional ellipsoid. They supported their experiments by potential flow arguments. Singh *et al.* (2005) performed experiments in a vacuum chamber on a flapping wing. Their results showed that the operating frequency attained by the mechanism was not the same as the frequency in air when supplying the same voltage to the driving mechanism. In order to evaluate the dependency of the added mass on the frequency of oscillations, it is important that the test frequencies in air and vacuum are closely matched. Brennen (1982) reviewed the state of knowledge, at that time, concerning the evaluation of the forces imposed on a body in a fluid due to acceleration of either the body or the fluid. He suggested that the added mass of a body of complex geometry might be estimated for each direction of acceleration from the principal dimensions of the projected area in that direction and a corresponding approximate formula.

In classical unsteady aerodynamic problems, the forces are usually split into those due to the relative acceleration between a moving body immersed in a fluid and circulatory effects induced by the vertical structure interaction associated with the wake (Theodorsen, 1935; Kussner, 1936; Von Karman, 1938). Such a separation is not very clear in some applications. For instance, oscillating a wing in still air may cause its flow patterns such as flow separation and vortex formation that would contribute to the pressure distribution over the wing. Because the added mass is related to the pressure distribution, one could expect significant departures of added mass values that are predicted by the classical potential flow theory.

The current literature does not include added mass values for wings oscillating at high frequencies as well as high angles of attack. To reduce this gap, we perform experiments to measure the aerodynamic loads on a wing section undergoing plunging oscillations over a frequency range between 18 and 100 rad/s and at angles of attack up to 50 degrees. We then estimate the forces associated with the added mass by subtracting the inertial loads from the measured force. In addition to providing experimental values for the added mass related with oscillating wings, we assess the dependence of the added mass on the frequency of the oscillations for different angles of attack by introducing the bicoherence analysis to investigate the quadratic nonlinearity coupling between three frequencies f_1, f_2 and their sum $f_1 + f_2$.

2. PROBLEM FORMULATION

2.1 Theoretical approach

When an airfoil undergoes oscillations in a fluid, additional pressure forces are required to accelerate the fluid in its vicinity (Leishman, 2006). These forces, which are referred to as the added mass effect, are functions of the local acceleration of the moving body. Based on Theodorsen's theory (Theodorsen, 1935), the non-circulatory force related to the added mass on a thin airfoil with a chord length $\bar{b}$ undergoing a plunging acceleration ($\ddot{h}$) is given by:

$$L_{added} = \rho\pi\bar{b}^2\,\ddot{h}\ . \tag{1}$$

As a background, the work done by Zakaria *et al.* (June 2015) illustrates the theoretical approach when the wing profile experience change in angle of attack, they consider the two-dimensional unsteady potential flow induced by an unsteady plunging motion, then the non-circulatory lift associated with a plunging airfoil can then be written as Kochin and Roze (1964):

$$L_{added} = [\rho\pi\bar{b}^2 cos^2(\alpha)\,\ell]\,\ddot{h}\ , \tag{2}$$

where α is the angle of attack. In our experiments, we consider a plunging motion having the form:

$$h(t) = h_a \sin(\omega t) = h_a \sin(2\pi f t)\ , \tag{3}$$

and define the maximum translation velocity of the plunging airfoil as the reference velocity, i.e. $U_{ref} = 2\pi f h_a$. A non-dimensional frequency based on a fixed ratio (h_a/c = 6.8%) can then be written as:

$$\widehat{F} = \frac{\omega c^2}{\nu}\ . \tag{4}$$

The plunging velocity and acceleration are given by:

$$\frac{dh}{dt} = \dot{h} = \omega h_a \cos(\omega t)\ , \tag{5}$$

and

$$\ddot{h} = -\omega^2 h_a \sin(\omega t)\ . \tag{6}$$

The theoretical plunging force obtained by accounting for both inertia and added mass of the wing is then given by:

$$Np_{theoretical} = [m_{moving} + \pi\rho\bar{b}^2 cos^2(\alpha)\ell\,]|\ddot{h}|\ . \tag{7}$$

2.2 Experimental approach

Assuming that the added mass is a function of the frequency and amplitude of the oscillations and the angle of attack, we write the most general expression

$$Np_{measured} = \big[m_{moving} + m_{added}(\omega, \alpha, h_a)\big]\omega^2 h_a\ . \tag{8}$$

This equation can be used to calculate the added mass from measured values of the aerodynamic loads as:

$$m_{added}(\omega, \alpha, h_a) = \frac{Np_{measured} - m_{moving}\,\omega^2 h_a}{\omega^2 h_a}\ . \tag{9}$$

3. Higher order spectral analysis

One of the very powerful tools is the higher-order spectrum analysis (HOS). It is the Fourier transform of the higher-order correlation. It identifies nonlinear interactions among frequency components and preserves the phase information, which is a more sensitive marker to detect the departure from linearity as compared to information related to amplitude (Dowell and UEDA, 1984). For a linear system, the second-order information embedded in a power spectrum represents the distribution of energy at different frequencies, which fully characterizes a linear system in the frequency domain. The normalized value of the cross-power spectrum captures the phase relation at the same frequency between two different signals. However, for nonlinear system higher-order spectrum is needed because the power spectrum cannot portray the energy transformation between the various frequency components which is a typical feature of nonlinear systems. Among these higher-order spectra, the bispectrum, the Fourier transform of triple correlation can capture quadratic nonlinearities. Further higher-order interactions can be tracked by trispectrum and beyond, but each additional order adds significantly to the computational demand and needs for a combined length of data sets (e.g., Kim and Powers (1979); Kareem and Gurley (1996); Hajj and Silva (2004)). A bispectrum is easy to visualize since it can be displayed as a bi-dimensional (2-D) plot, whereas, further higher-order spectra can be only viewed in 3-D plot by slicing the hyper-dimension at different frequencies.

To remove the dependence on the amplitudes of the frequencies, the bispectrum is normalized by these amplitudes to obtain the bicoherence. If the bicoherence is equal to 1 the system are quadratically coupled, if it is equal to 0, then the system is not quadratically coupled and if the system is partially coupled the bicoherence is between 0.0 < bicoherence < 1.0 (Hajj *et al.*, 1993). The Figure 1 shows the schematic 2-D bicoherence plot, the results are displayed inside the triangle and f_N is the Nyquist frequency, more details can be found by (Hajj *et al.*, 1997).

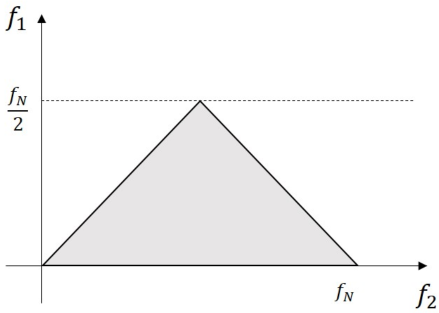

Figure 1. Symmetry properties of the bispectrum, (f_N: Nyquist frequency).

3.1 Frequency response function

The ultimate goal in the analysis of a collection of sample records is often is to establish a linear relationship between the data represented by various records. The existence of this relationships can be detected for cross correlation, cross-spectral density or coherence function estimates. However, a meaningful description of the linear relationships is best provided computing the frequency response functions of the relationships, as indicated by Block H.

$$\widehat{H}(f) = \frac{\widehat{G}_{xy}(f)}{\widehat{G}_{xx}(f)} = |\widehat{H}(f)|e^{-j\widehat{\phi}(f)} \tag{10}$$

It follows that we can write the gain as,

$$|\widehat{H}(f)| = \frac{|\widehat{G}_{xy}(f)|}{\widehat{G}_{xx}(f)} \tag{11}$$

and the phase,

$$\widehat{\phi}(f) = \widehat{\theta}_{xy}(f) \tag{12}$$

where $\widehat{G}_{xx}(f)$ and $\widehat{G}_{yy}(f)$ are the estimated auto-spectral density functions of x(t) and y(t) respectively, and $\widehat{G}_{xy}(f)$ is the estimated cross-spectral density functions between x(t) and y(t). Figure 2 presents the proposed block diagram that describes the dynamics of the input plunging motion.

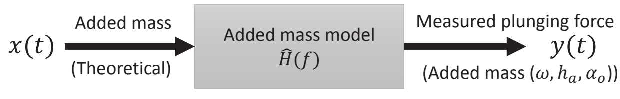

Figure 2. The proposed transfer function block diagram.

In such dynamical system, the input function appears to be the theoretical value of the added mass force given in eq.2. The output function is the measured forces recorded by the strut mount, as such, we proposed these obtained forces to be a new definition for the added mass as function of frequency, plunging amplitude and angle of attack.

4. EXPERIMENTAL TESTING

The experiments were conducted in an open jet wind tunnel. The wing section profile is that of a NACA-0012. The wing section was composed of a foam core structure reinforced with a solid carbon fiber rod at the quarter chord location. The wing was fabricated from laminated carbon-fiber strips (foam cored) that were covered with a thin finish epoxy film sheet. The wing section has a chord length of $0.14m$ and a span of 0.63 m.

Figure 3 shows a schematic of the airfoil motion kinematics. End plates were attached to the wing tip to reduce the three-dimensional flow effects that would otherwise originate from these tips. Two MEMS accelerometers were placed on the bracket that held the wing. In all performed experiments, the maximum displacement of the plunge motion was maintained constant at a value of h_o =0.0193 m and the geometric reduced frequency was calculated to be $k = c/2h_a = 0.14/0.0193 = 7.253$. The moving mass contributing to the inertial force was calculated to be $0.477kg \pm 1grams$.

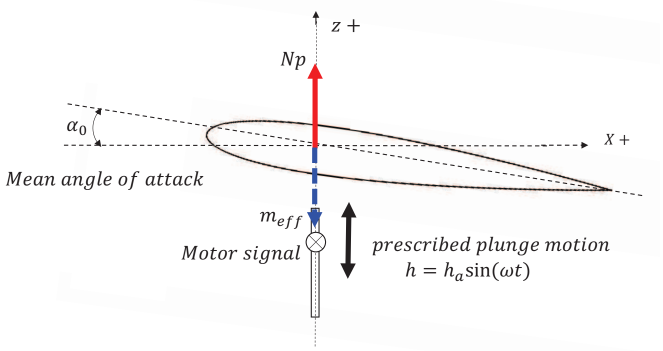

Figure 3. Airfoil prescribed motion kinematics

The acceleration of the wing was measured using two MEMS accelerometers. The operating angle of attack of the wing was measured using a digital protractor with an accuracy of $\pm$ 0.2 degrees. The force measurements were obtained by using a strut mount (6-component balance) and the data was acquired using National Instruments SCXI-1520 system sampled at 2500 Hz and low-pass filtered at 55 Hz using a fourth order butter-worth low-pass filter. The wing aeroelastic effect was addressed using high CCD camera to measure the tip deflection at the highest operating frequency and was found to be 0.05% of the plunging amplitude when operating at a frequency of 100 rad/s as shown in Figure 4. For further details for the experiments, the reader should refer to Zakaria *et al.* (Jan 2015) reference.

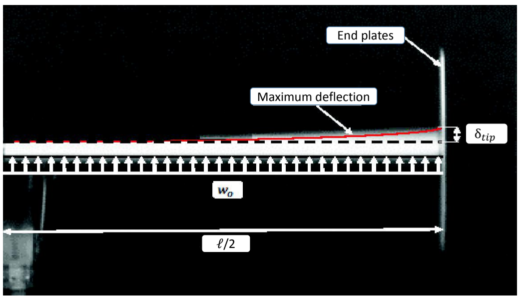

Figure 4. High-speed photogrammetry image of the wing at 100 rad/s forced oscillatory motion.

5. RESULTS AND DISCUSSION

The added mass effect was identified using two methods. The first method was based on a force balance equation where the measured plunging forces is equal to the actual moving mass and apparent mass contributions function of airfoil shape, angular velocity and plunging amplitude. The second method was based on the power spectra of the measured plunging forces at each operating frequency and mean angle of attack, which is used to get the relation between the output amplitude of the total force measured divided by the input theoretical added mass forces. Using the Eq. 9 one can measure the apparent mass effect while increase the angle of attack and the frequency, which should and appear to approach the theoretical potential flow value at low frequencies. Thus, we postulate that the curve fit for the added mass coefficient $C_a = m_a/\rho\pi\bar{b}^2\ell$ should approach its theoretical value of $\cos^2\alpha$ as $\omega \to 0$. A linear curve fit to the measured added mass as defined by Eq. 9, is then written as:

$$C_a = \frac{m_a}{\rho\pi\bar{b}^2\ell} = \cos^2\alpha + C\frac{c^2\omega}{\nu}\ . \tag{13}$$

Figure 5 shows linear curve fits of the added mass coefficient (added mass normalized with $\rho\pi\bar{b}^2\ell$) as a function of the oscillation frequency for different angles of attack and different plunging frequencies. Although the data show significant scatter, there is clear evidence that the added mass increases as the frequency of the oscillation is increased. One observation from the Fig. 5 is that the deviation from theoretical results shows significant forces that could be attributed to flow patterns such as the interaction with leading and trailing edge vortices.

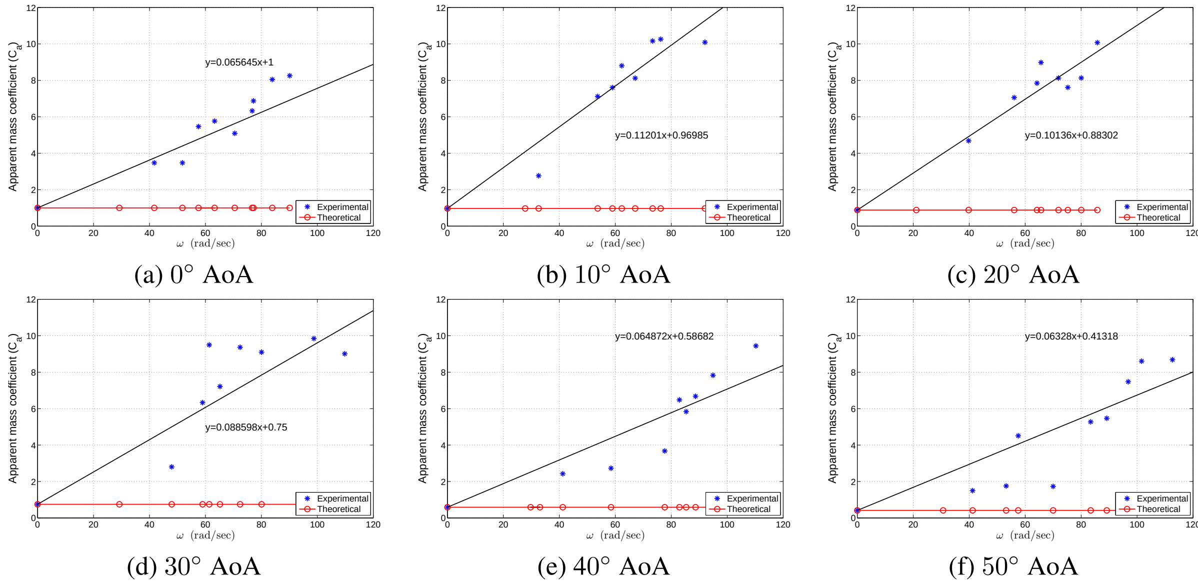

(a) 0° AoA (b) 10° AoA (c) 20° AoA

(d) 30° AoA (e) 40° AoA (f) 50° AoA

Figure 5. Measured apparent mass at different operating frequencies and angles of attack

Figure 6 shows the 3D analysis of the power spectrum for all angles of attack, where the dotted curve is the force measured by the balance (Np measured) and the solid line is the predicted input power calculated using the acceleration (Np theoretical). We observed the appearance of the super harmonics at all cases, and these super harmonics indicate the presence of nonlinearities in the system. Thus, an analysis were done by HOS through the bi-spectrum plots to identify if there is nonlinear quadratic coupling.

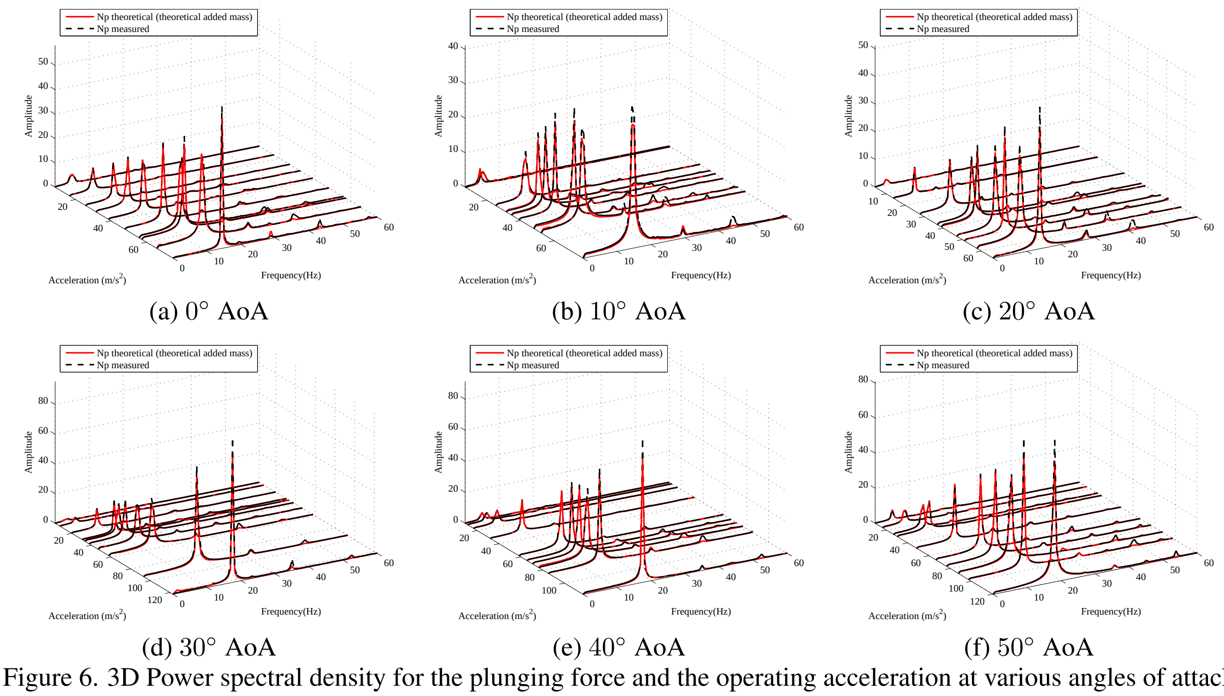

(a) 0° AoA (b) 10° AoA (c) 20° AoA

(d) 30° AoA (e) 40° AoA (f) 50° AoA

Figure 6. 3D Power spectral density for the plunging force and the operating acceleration at various angles of attack

Figures 7 and 8 show the bi-spectrum for two different cases: (i) The system when the fundamental frequency (f_0) is 12.50 Hz at zero angle of attack, (ii) The fundamental frequency equal to 11.25 Hz and 50 degrees of angle of attack. The bicoherence show peaks are centered at (f_0,f_0) and at ($2f_0$, f_0), which indicates the forcing of the first and second harmonics band, which is clearly visible in the power spectra (Fig. 8(a)). The other peaks suggest that adjacent instability modes interact to produce the another super harmonics, the cut-off is determined at 0.8. The high bicoherence values at $(f_0, 4f_0)$ indicate that the sum modes are also coupled with the difference fluctuations. One can see that there are some difference between the results, looking for the Fig. 8, when the angle of attack is 50^o, note that the effect of nonlinearity is more intense for the entire spectrum, especially for higher frequencies, so the generating source of nonlinearity is more intense in this case. In the bicoherence contour plot, one can observe that the phase coupling between the fundamental harmonic with itself generates the first $(11.25Hz + 11.25Hz = 22.50Hz)$ and other super harmonics.

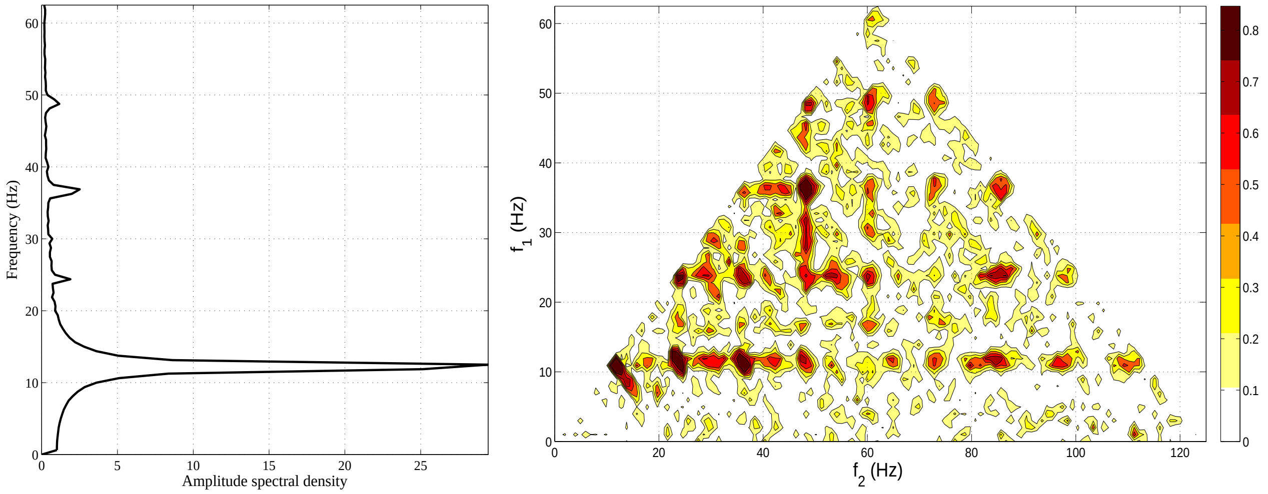

(a) Power spectrum density

(b) Auto-bicoherence (cut-off of 0 to 1)

Figure 7. HOS analysis for the zero angle of attack and 12.5 Hz.

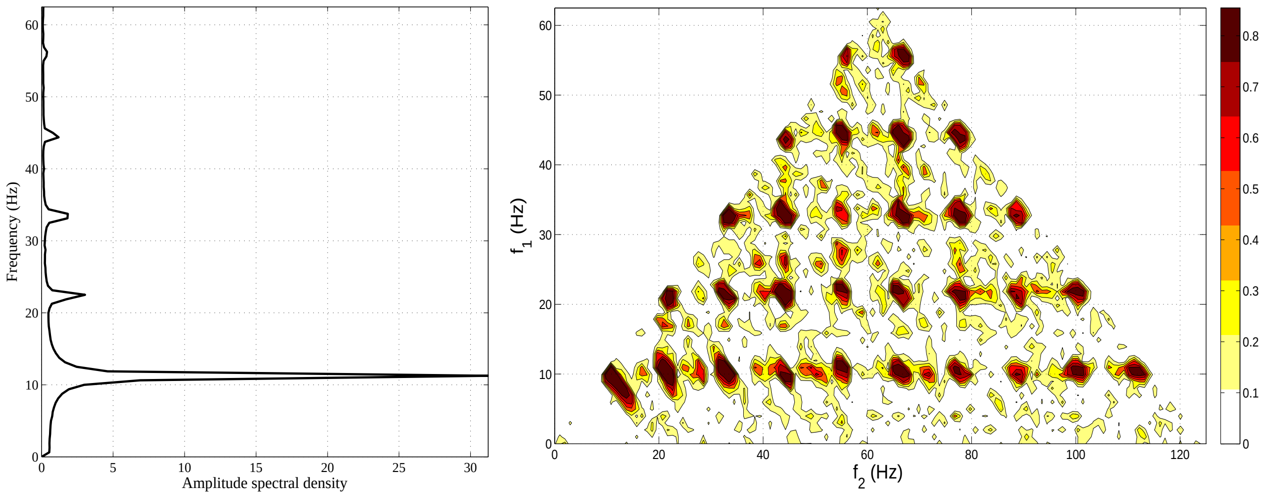

(a) Power spectrum density

(b) Auto-bicoherence (cut-off of 0 to 1)

Figure 8. HOS analysis for 50 degrees in the angle o attack and 11.25 Hz.

Figure 9 shows the magnitude and the phase at $0°$, $10°$, $40°$ and $50°$ for the preset angles of attack, based on the response function found in eq.10. The gain function shows a second order behavior for all angles of attack. One can see the first resonance pick at the fundamental frequency, however, it clearly the presence of another harmonics at high frequencies that can be connected with the appearance of the nonlinearities. We also observed a gain peak for $0°$ and $10°$ angles of attack at $12Hz$, and for $40°$ and $50°$ at $15Hz$, respectively. The phase between the input and output are $-72°$ and $-83°$ for $0°$ and $10°$ angles of attack; $125°$ and $143°$ for $40°$ and $50°$ angles of attack, those results show a changing in the phase relation when the system presents high angles of attack.

6. CONCLUSIONS

The results presented in this work provide measured data of forces associated with the added mass on an airfoil undergoing plunging oscillations at high frequencies and high angles of attack. This variation indicates that the added mass is linearly dependent on this frequency. The results also show that the added mass is largest for angles of attack

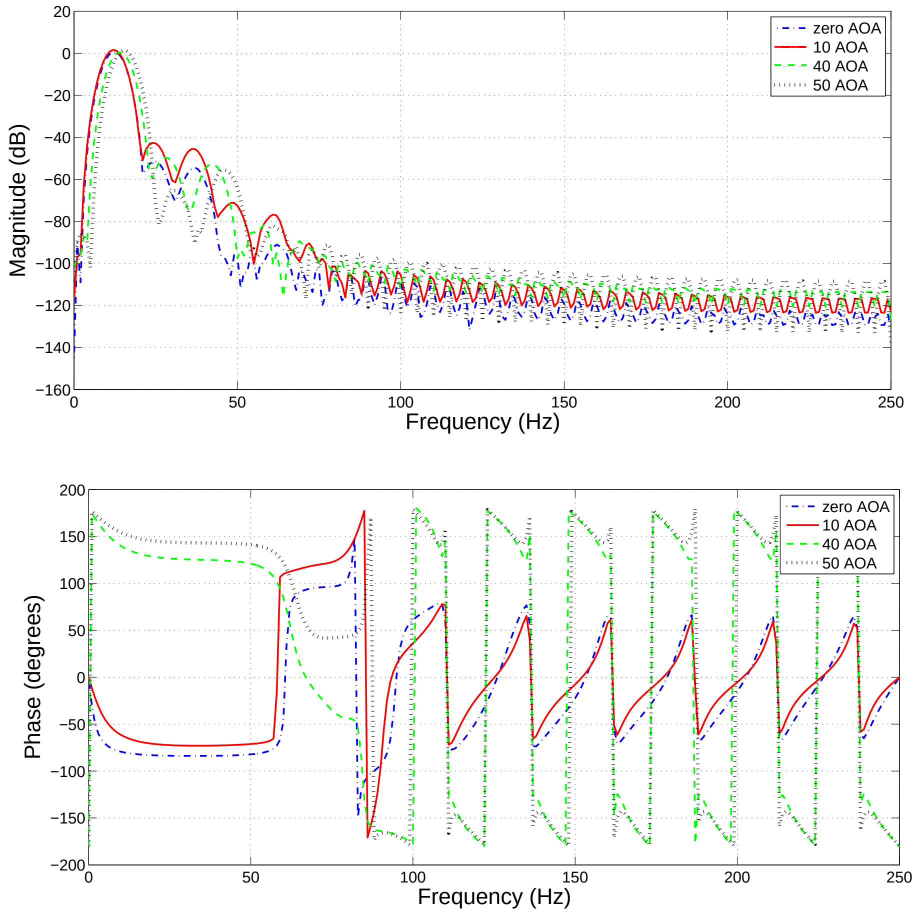

Figure 9. Frequency response function for the added mass forces.

between 10° and 20° and lowest for angles of attack between 40° and 50°. The dependence of the added mass on the frequency of the oscillations and the angle of attack indicate a significant effect of the flow vortices interaction generated by the oscillating airfoil. The contribution to the added mass as calculated here was demonstrated by higher order spectral analysis. The results show that there is a strong sub-harmonic coupling at 50°, consequently, we can attribute this strong coupling as leading and trailing vortex interactions between different time scales.

7. ACKNOWLEDGMENTS

The first author thanks Dr Saad Ragab at Virginia Tech for his physical interpretation in the theoretical approach.

8. REFERENCES

Brennen, C., 1982. "A review of added mass and fluid inertial forces".

Dowell, E. and UEDA, T., 1984. "Flutter analysis using nonlinear aerodynamic forces". *Journal of Aircraft*, Vol. 21, No. 2, pp. 101–109.

Granlund, K. and Simpson, R., 2007. "Modeling unsteady maneuvers of slender bodies". *AIAA Paper*, Vol. 6721, p. 2007.

Hajj, M., Miksad, R. and Powers, E., 1993. "Fundamental–subharmonic interaction: effect of phase relation". *Journal of Fluid Mechanics*, Vol. 256, pp. 403–426.

Hajj, M., Miksad, R. and Powers, E., 1997. "Perspective: Measurements and analyses of nonlinear wave interactions with higher-order spectral moments". *Journal of fluids engineering*, Vol. 119, No. 1, pp. 3–13.

Hajj, M.R. and Silva, W.A., 2004. "Nonlinear flutter aspects of the flexible high-speed civil transport semispan model". *Journal of aircraft*, Vol. 41, No. 5, pp. 1202–1208.

Kareem, A. and Gurley, K., 1996. "Damping in structures: its evaluation and treatment of uncertainty". *Journal of Wind Engineering and Industrial Aerodynamics*, Vol. 59, No. 2, pp. 131–157.

Kim, Y.C. and Powers, E.J., 1979. "Digital bispectral analysis and its applications to nonlinear wave interactions". *Plasma Science, IEEE Transactions on*, Vol. 7, No. 2, pp. 120–131.

Kochin, Nikola Evgrafovich, A.K.I. and Roze, 1964. *Theoretical hydromechanics*. Interscience.

Kussner, H., 1936. "Untersuchung der bewegung einer platte beim eintritt in eine strahlgrense". *Luftfahrt forschung*, Vol. 13, No. 425.

Leishman, J.G., 2006. *Principles of helicopter aerodynamics*. Cambridge University Press.

Maniaci, D.C. and Li, Y., 2011. *Investigating the influence of the added mass effect to marine hydrokinetic horizontal-axis turbines using a General Dynamic Wake wind turbine code*. IEEE.

Singh, B., Ramasamy, M., Chopra, I. and Leishman, J.G., 2005. "Insect-based flapping wings for micro hovering air vehicles: experimental investigations". In *American Helicopter Society International Specialists Meeting on Unmanned Rotorcraft, Phoenix, AZ*. pp. 18–20.

Theodorsen, T., 1935. "General theory of aerodynamic instability and the mechanism of flutter". Technical Report 496, NACA.

Von Karman, T., 1938. "Airfoil theory for non-uniform motion". *Journal of the Aeronautical Sciences (Institute of the Aeronautical Sciences)*, Vol. 5, No. 10, pp. 379–390.

Zakaria, M.Y., Pereira, D.A., Ragab, S.A., Hajj, M.R. and Marques, F.D., June 2015. *An Experimental Study of Added Mass on a Plunging Airfoil Oscillating with High Frequencies at High Angles of Attack*, American Institute of Aeronautics and Astronautics, Vol. AIAA 2015-3166 of *33rd AIAA Applied Aerodynamics Conference, AIAA Aviation Conference proceeding, Texas, Dallas, USA*.

Zakaria, M.Y., Taha, H.E. and Hajj, M.R., Jan 2015. "Experimental investigations of the lift frequency response at high angles of attack". *AIAA Scitech Conference proceeding, Kissimmee, Florida, USA*, Vol. AIAA paper 2015-1503, pp. PP (1–18).

9. RESPONSIBILITY NOTICE

The authors are the only responsible for the printed material included in this paper.